Received: 7 September 2021 | Revised: 27 October 2021 | Accepted: 28 October 2021

DOI: 10.1002/bit.27981

ARTICLE

BIOTECHNOLOGY AND BIOENGINEERING WILEY

Engineering human liver fatty acid binding protein for detection of poly- and perfluoroalkyl substances

Madison M. Mann | James D. Tang | Bryan W. Berger

Department of Chemical Engineering, University of Virginia, Charlottesville, Virginia, United States

Correspondence
Bryan W. Berger, Department of Chemical Engineering, University of Virginia, Charlottesville, VA 22904 USA.
Email: bryan.berger@virginia.edu

Funding information
National Institute of General Medical Sciences, Grant/Award Number: T32GM136615

Abstract

Per- and polyfluoroalkyl substances (PFAS) are a large group of synthetic fluorinated chemicals with surface active and water-repellent properties. The combination of wide-spread use in numerous consumer and industrial products and extended biological half-lives arising from strong carbon–fluorine bonds has led to significant accumulation of PFAS in humans. As most human interaction with PFAS comes from ingestion, it is important to be able to detect PFAS in drinking water as well as in agricultural water. Here we present an approach to designing a fluorescence-based biosensor for the rapid detection of PFAS based on human liver fatty acid binding protein (hLFABP). Introduction of solvatochromic fluorophores within the ligand binding pocket (L50) allowed for intrinsic detection of perfluorooctanoic acid (PFOA), perfluorooctanesulfonic acid (PFOS), and perfluorohexanesulfonic acid (PFHxS) via blue-shifts in fluorescence emission spectra. Initially, a single tryptophan mutation (L50W) was found to be able to detect PFOA with a limit of detection (LOD) of 2.8 ppm. We improved the sensitivity of the biosensor by exchanging tryptophan for the thiol reactive fluorophore, acrylodan. The acrylodan conjugated C69S/F50C hLFABP variant is capable of detecting PFOA, PFOS, and PFHxS in PBS with LODs of 112 ppb, 345 ppb, and 1.09 ppm, respectively. The protein-based sensor is also capable of detecting these contaminants at similar ranges in spiked environmental water samples, including samples containing an interfering anionic surfactant sodium dodecyl sulfate. Overall, this study demonstrates engineered hLFABP is a useful platform for detection of PFAS in environmental water samples and highlights its ease of use and versatility in field applications.

KEYWORDS
biosensor, fatty acid binding protein, fluorescence, protein engineering, substrate specificity, tryptophan

1 | INTRODUCTION

Per- and polyfluoroalkyl substances (PFAS) have become increasingly notorious environmental contaminants and a growing public health concern. This large group of chemicals contain hydrophobic, highly fluorinated carbon chains (C_6–C_{10}) and terminal hydrophilic headgroups. These headgroups are typically comprised of carboxylic acids or sulfates, which impart unique interfacial properties such as the ability to repel oils and water. As a result, PFAS are abundant in everyday items including stain and water-resistant fabrics, nonstick cookware, and even hygienic products like dental floss (Favreau et al., 2017; Kotthoff et al., 2015; Robel et al., 2017; Schaider et al., 2017; Wang et al., 2017). Additionally, aqueous film-forming foams containing PFAS have been used for decades at airports as

well as various manufacturing facilities where highly flammable fuel or solvents are stored (Dauchy et al., 2017).

Among PFAS compounds, the medium chain perfluorooctanoic acid (PFOA) and perfluorooctanesulfonic acid (PFOS) are most commonly found in the environment. Over the last decade, medium-chain polyfluoroalkyl compounds have been replaced by shorter-chain alternatives like perfluorohexanesulfonic acid (PFHxS). However, these short-chain derivatives have also been implicated in environmental bioaccumulation and toxicity on par with their longer-chain counterparts (Butt et al., 2014; Harding-Marjanovic et al., 2015). Once in the environment, PFAS compounds end up in groundwater, soils and biosolids. The United States Environmental Protection Agency has set drinking water advisory levels at 70 ppt for PFOA and PFOS combined (United States Environmental Protection Agency Office of Water 4304T Health and Ecological Criteria Division, 2016a, 2016b). However, in areas where major PFAS release has occurred, individual concentrations of PFOS and PFOA in surface and groundwater have been detected between 100 and 1000 times that of recommended levels (Carlson & Tupper, 2020; Cousins et al., 2016; Dauchy et al., 2019). In leafy greens and other vegetables grown in contaminated areas, accumulation of PFAS can reach 1 mg/kg of dry weight (Blaine et al., 2013, 2014). As a result, most people are exposed daily to PFAS in drinking water and food; according to recent data from the Centers for Disease Control and Prevention, PFAS (including PFOA and PFOS) were detected in the serum of all survey participants at ng/ml levels (Calafat et al., 2006, 2007).

Prolonged exposure to PFAS has been linked to several negative health effects (Fenton et al., 2021), including increased cholesterol levels (Steenland et al., 2009, 2010), liver and kidney disease (Armstrong & Guo, 2019; Stanifer et al., 2018) as well as impairment of the immune system. Recent studies have suggested high levels of PFOA are correlated with reduced vaccine response (Abraham et al., 2020; Looker et al., 2014), and chronic exposure to PFAS could render a person more susceptible to pathogens or viral infections (Bulka et al., 2021). PFAS has been shown to transfer from mother to fetus (Mamsen et al., 2019), and prenatal exposure to PFAS has been linked to low birth weight (Washino et al., 2009), neurobehavioral issues (Hoffman et al., 2010; Vuong et al., 2016), as well as childhood adiposity (Mora et al., 2017, 2018).

The current standard for detection of PFAS is via liquid and gas chromatography coupled with mass spectrometry Shoemaker (2020). This method is highly sensitive, capable of detecting parts per trillion (ppt) levels depending on the type of sample matrix being tested. These methods also requires highly sophisticated equipment and training, and therefore is not readily available for widespread, rapid use in testing foods, commercial products or water samples (Hu et al., 2020; Shoemaker, 2020). Given the diversity of PFAS contaminated materials, the range of concentrations necessary for testing, and desire for portable and flexible testing, there is an increasing need to develop rapid and robust methodologies for PFAS detection. Most PFAS technologies rely on complexation with organic dyes, allowing for optically based detection. Specifically, complexation of PFAS with a cationic dye has been utilized to develop an app-based test kit for PFOS (Fang et al., 2018). While this technology is portable and offers detection on the order of parts per billion (ppb), prior clean-up steps in the form of liquid or solid phase extraction are required as interference of inorganic ions like chloride inhibit detection (Fang et al., 2018). Molecularly imprinted polymers (MIPs) and immunoassays are other promising PFAS sensors with significantly lower limits of detections (Feng et al., 2014; Jiao et al., 2018; Karimian et al., 2018). A chitosan MIP doped with carbon quantum dots allows for the fluorescent detection of PFOS in the ppt range as the contaminant interacts with cavities previously imprinted with the targeted analyte (Jiao et al., 2018). However, the fluorescent capabilities of this MIP are limited to their specifically targeted analytes; while MIPs are most often used for their high sensitivity and selectivity, they are unable to simultaneously detect multiple PFAS compounds in a mixture. Recent MIP work using electrochemical detection was able to demonstrate high sensitivity for PFOS, but unable to distinguish it from other PFAS compounds (Kazemi et al., 2020). Additionally, immunoassays take advantage of receptor–ligand interactions, for example peroxisome proliferator-activated receptor alpha response elements were modified with gold nanoparticles to detect PFOS at ppt levels using optical density changes (Xia et al., 2011). While promising, immunoassays can be challenging to implement in field applications due to the time, infrastructure, and reagents required for multiple washing and incubation steps before detection, as well as a need for pretreatment to remove potentially interfering compounds in complex mixtures.

In contrast to synthetic scaffolds such as nanoparticles or polymers, engineered proteins can be tuned for selectivity and affinity for a given ligand from complex mixtures (e.g., environmental samples) and can incorporate fluorescence and other highly sensitive optical detection methods. One such potential protein scaffold is the human liver fatty acid binding protein (hLFABP), a cytosolic protein expressed in the liver, kidneys, and intestines (Atshaves et al., 2010) whose expression has been shown to be upregulated in response to PFOA exposure (Sheng et al., 2018). LFABP contains a large hydrophobic β barrel binding region composed of antiparallel β sheets with two α helices covering one end creating a helix-turn-helix (HTH) motif (Sharma & Sharma, 2011; Thompson et al., 1997). This well-defined β barrel motif is typical of other fatty acid binding proteins, but LFABP is unique in its ability to bind two cognate ligands (Sharma & Sharma, 2011; Thompson et al., 1997).

PFAS, particularly perfluoroalkyl acids, share a structural similarity to the natural ligands of LFABP. In an attempt to understand toxicity and bioaccumulation, others have shown that PFAS can bind to the protein in a similar manner as native fatty acid ligands (Sheng et al., 2016). Also, the native forms of both rat and human LFABP binds PFOA and PFOS as well as short-chain PFHxS with moderate affinity and micromolar dissociation constants (K_d) (Cheng & Ng, 2018; Sheng et al., 2016).

In this study, we describe a strategy to reengineer hLFABP as a scaffold for PFOA, PFOS, and PFHxS detection via the introduction of solvatochromic fluorophores into the protein's ligand binding pocket. Using a structure-guided approach, we identified key

mutations in the inner binding pocket that are sensitive to PFAS ligand binding as a function of chain length and demonstrated binding using intrinsic tryptophan fluorescence. By modifying one such residue (Phe50) with the solvatochromic fluorophore, 6-acryloyl-2-dimethylaminonaphthalene [acrylodan], we significantly increased the limit of detection (LOD) to ppb levels. Furthermore, we demonstrate robustness to and specificity of PFAS ligand binding in surface water samples, and in samples spiked with the anionic surfactant, sodium dodecyl sulfate (SDS), which can compete with PFAS binding. Collectively, our results indicate that hLFABP can be reengineered to significantly improve detection for PFAS ligands and suggests possible improvements for further detection of this challenging and important class of environmental toxins.

2 | MATERIALS AND METHODS

2.1 | Molecular biology

An *E. coli* codon optimized form of hLFABP (NCBI 2168) was synthesized and subcloned into the pET-28a(+) vector using BamHI/XhoI restriction sites (GenScript). The gene includes N- and C-terminal hexahistidine tags. Unless otherwise stated, all other molecular biology procedures for PCR amplification, plasmid preparation, cell transformation, and subcloning were performed according to standard methods supplied by manufacturers. For site-directed mutagenesis, primers were designed using PrimerX, and mutations were introduced using the QuikChange II site-directed mutagenesis kit (Agilent). Mutated sequences were verified by DNA sequencing (GeneWiz). For DNA maintenance, *E. coli* strain DH5α was used and for protein expression *E. coli* strain BL21 (DE3) was used.

2.2 | Protein expression and purification

Transformed *E. coli* BL21 cells were grown to saturation in 10 ml of LB containing kanamycin (50 μg/ml) overnight at 37°C with 200 rpm agitation. The next day, cells were pelleted by centrifugation (3000*g*), and resuspended in fresh media containing kanamycin. The suspension was grown to an OD of 0.7 at 37°C. Protein expression was then induced via addition of 1 mM isopropyl β-D-1-thiogalactopyranoside (IPTG), and cultures transferred to 20°C. Cells were harvested after an 18-h growth by centrifugation (12,000*g*) and resuspended in lysis buffer (50 mM Tris-Cl, 100 mM NaCl, 5% v/v glycerol) before lysis via sonication. The lysis mixture was clarified by centrifugation (12,000*g*), and the insoluble fraction discarded.

The supernatant containing soluble protein was then separated by affinity chromatography on a 1 ml HisTrap HP column using an AKTA Pure system (GE Healthcare). The column was equilibrated with 50 mM Tris-Cl buffer (pH 8) containing 10 mM imidazole, and protein was separated using a stepwise elution of imidazole up to 500 mM. The fractions collected were analyzed by SDS-PAGE to determine purity. Pure hLFABP containing fractions were pooled and dialyzed against 50 mM Tris-Cl buffer (pH 8) or phosphate-buffered saline (PBS) buffer (pH 7.5).

Delipidation of the protein was performed at 37°C using hydroxyalkoxypropyl-dextran (Sigma-Aldrich), a Lipidex-5000 equivalent resin. Resin was equilibrated with buffer for 1 h at 37°C before sample was applied and incubated for 2 h at 37°C with gentle agitation. Protein samples were collected after centrifugation and filtration through a 0.2 μm filter. Concentration of all protein samples was measured using a Pierce BCA protein assay kit.

2.3 | Acrylodan labeling

Acrylodan labeling reactions containing 20 mM protein, 50 mM acrylodan, and 8 M urea in 5 ml of PBS (pH 7.5) were incubated at room temperature for 10 h with gentle mixing. Removal of unreacted acrylodan and refolding of denatured protein was performed on-column with a gradient from 8 to 0 M urea in 50 mM Tris-HCl buffer (pH 8) containing 10 mM imidazole. The protein was then eluted using 500 mM imidazole containing buffer, pooled, and dialyzed into PBS buffer overnight. The degree of labeling was determined by measuring the protein concentration using a BCA protein assay, as well as acrylodan concentration measured by absorption at 370 nm (extinction coefficient 16,400 $M^{-1}\,cm^{-1}$) (Prendergast et al., 1983). Degree of labeling for C69S/F50C hLFABP was 1.0.

2.4 | Fluorescence displacement assays

Binding of the fluorophore 1-anilinonaphthalene-8-sulfonic acid (ANS) to hLFABP was performed in a similar manner as described previously to obtain max fluorescence intensity for the complex (Velkov et al., 2005). Briefly, hLFABP (1 μM) in either 50 mM Tris buffer containing 1 mM BME or PBS buffer (pH 7.5) was titrated with ANS (0–50 μM). After an equilibration time of 5 min, fluorescence emission spectra between 420 and 600 nm as well as end point intensity at 470 nm were collected with excitation at 400 nm. The data were corrected for background free protein and ANS fluorescence.

The maximum fluorescence upon saturation of fluorophore (F_{max}) as well as the dissociation constant ($K_{d,ANS}$) were determined by fitting the fluorescence intensity (F) and corresponding concentration of ANS ([ANS]) to a one-site binding model using nonlinear regression:

$$F = F_{max} \times \frac{[ANS]}{(K_{d,ANS} + [ANS])}.$$

This $K_{d,ANS}$ value is equivalent to the concentration of free fluorophore in the system at half the maximum fluorescence, and was used to calculate the inhibition constant (K_i) of PFAS for the proteins.

The binding of PFAS to hLFABP variants was measured by displacement of bound ANS. hLFABP (2 μM) was first equilibrated with ANS (100 μM) in excess for 5 min. PFAS was then titrated into

hLFABP-ANS samples resulting in a final protein concentration of 1 μM. After a 5-min incubation, fluorescence emissions spectra were collected between 420 and 600 nm with excitation at 400 nm. Measurements were corrected using blanks containing the ANS-hLFABP complex as well as protein in buffer only.

The displacement of ANS was characterized as the percent loss in fluorescence and was calculated as the decrease in area under the emission spectra for various PFAS concentrations. The concentration of PFAS necessary to displace half of the bound ANS and inhibit fluorescence by 50% (IC_{50}) was found by fitting displacement data to a sigmoidal dose–response curve where F_{min} and F_{max} represent the maximum and minimum ANS displacement by PFAS respectively:

$$\%\text{Initial fluorescence} = F_{min} + \frac{(F_{max} - F_{min})}{(1 + 10^{((\log(IC_{50}) - \log([PFOA]) \times HS)}).}$$

The inhibition constants (K_i) were then found by relating the value to the half maximal inhibitory constants (IC_{50}) and the dissociation constant for ANS in the absence of PFAS ($K_{d,ANS}$).

$$K_i = \frac{IC_{50}}{\frac{[ANS]_{total}}{K_{d,ANS}} + 1}.$$

2.5 | Circular dichroism

hLFABP variant C69S/F50C unlabeled and labeled with acrylodan were diluted to 10 μM in 50 mM sodium phosphate buffer (pH 7.5). Circular dichroism spectra were obtained in a quartz cuvette (0.1 cm) at 20°C using a Jasco J-1500 CD spectrometer from 250 to 190 nm. Reported spectra are averages of four scans and are expressed in terms of mean residue ellipticity (MRE) (deg cm^2/dmol). MRE values are based on a mean residue weight of 112 and 113 for unlabeled and acrylodan labeled C69S/F50C hLFABP, respectively. The content of structural elements were estimated using the web based server BeStSel (Micsonai et al., 2018).

2.6 | Equilibrium fluorescence titration assays

All fluorescence measurements for wild-type (WT) hLFABP and variants were performed using a Synergy Neo2 Hybrid Multi-Mode Microplate Reader (Biotek) at room temperature and under steady state conditions.

Initial PFOA binding assays were performed by titrating up to 1000 μM PFOA into WT hLFABP and tryptophan containing variants (L28W, F50W, F18W, F63W) in 50 mM Tris-Cl buffer (pH 8). After a 5-min incubation, fluorescence spectra were recorded for a wavelength range of 300–400 nm after excitation at 280 nm.

For the acrylodan labeled C69S/F50C hLFABP variant, PFAS binding assays were performed by titrating PFAS into 1 μM protein in either PBS buffer (pH 7.5) or creek water. To determine sensor ability in systems containing other anionic surfactants, the assay was also performed in PBS buffer (pH 7.5) with SDS at a final concentration of 1 μM. Samples were allowed to equilibrate for 5 min before fluorescence spectra were recorded over 420–600 nm after excitation at 395 nm.

To quantify averaged shifts in fluorescence spectra after ligand binding, the center of mass was calculated for each curve using the following equation: For tryptophan fluorescence, the peak center of mass was calculated over a wavelength (l) range of 300–400 nm while a range of 420–600 nm was used for acrylodan.

$$x_{cm} = \frac{\sum_{i=\lambda 1}^{\lambda 2} l_i x_i}{\sum_{i=\lambda 1}^{\lambda 2} l_i}.$$

3 | RESULTS AND DISCUSSION

Tryptophan fluorescence is extremely sensitive to environmental polarity, and is often used as an intrinsic probe for the study of protein conformational changes and ligand binding (Markiewicz et al., 2016; Royer, 2006) hLFABP contains no natural tryptophan residues. Prior work has shown that replacing a leucine residue in the outer binding pocket with tryptophan (L28W) creates a mutant sensitive to natural fatty acid ligand binding (Hagan et al., 2005). Therefore, single tryptophan mutations within the inner and outer ligand binding pockets were introduced as probes for PFAS binding, and residues chosen for mutation are shown in Figure 1 (Cai et al., 2012).

Several tryptophan containing hLFABP variants were created, including L28W as well as conservative phenylalanine to tryptophan mutations along the inner binding pocket (F50W and F63W). These mutations were chosen based on proximity to natural ligands as shown in Figure 1. While neither L28W and F63W showed changes in emission nor fluorescence intensity upon PFOA binding, one mutant (F50W) exhibited blue-shifted emission spectra upon titration of PFOA as shown in Figure 2a. This suggests that upon PFOA binding, aqueous solvent is displaced within the inner binding pocket and the

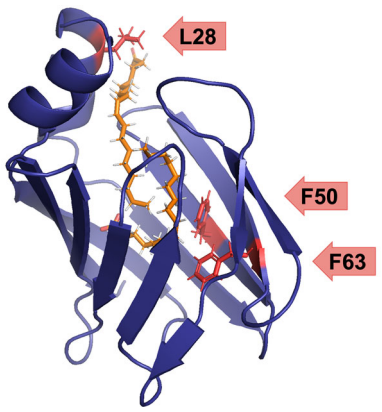

FIGURE 1 hLFABP in complex with two oleic acid molecules. The residues chosen for mutation (L28, F50, F63) are highlighted in red. Figure created using PyMOL (PDB: 2LKK). hLFABP, human liver fatty acid binding protein

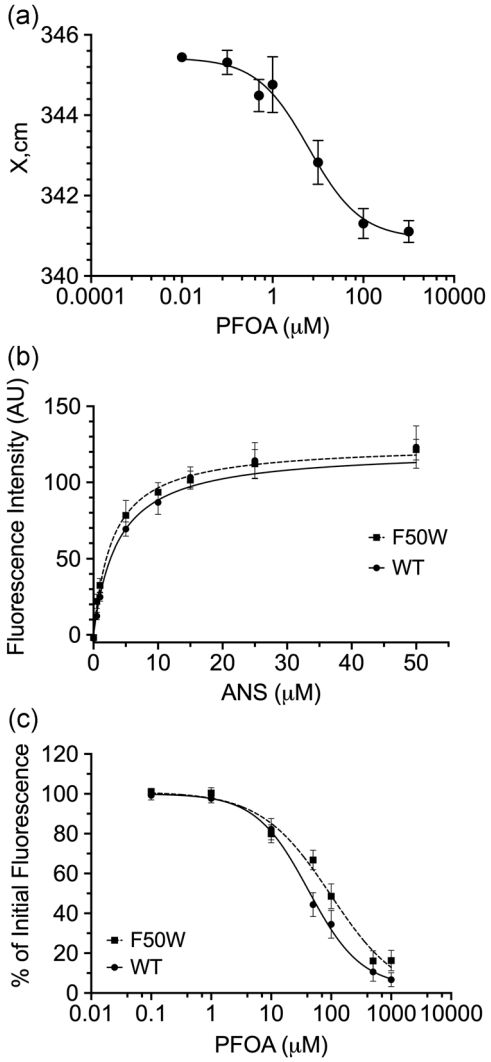

FIGURE 2 (a) Weighted average center of mass (*X*, cm) of fluorescence spectra for F50W hLFABP (10 μM) after titration with PFOA. (b) Binding of 1,8-ANS to WT and F50W hLFABP (1 μM) characterized using relative fluorescence intensity as a function of fluorophore (1,8-ANS) concentration. The data were fit to a one-site binding model using Prism. The represented points are mean values ± SE with $n = 3$. (c) Fluorescence decrease, quantified as the % of initial fluorescence for PFOA. Data were fit to a dose–response model using Prism. The represented points are mean values ± SE with $n = 3$. 1,8-ANS, 1-anilinonaphthalene-8-sulfonic acid; hLFABP, human liver fatty acid binding protein; PFOA, perfluorooctanoic acid; WT, wild type

polarity of the microenvironment surrounding F50W is decreased. This reduction in polarity decreases solvent relaxation of the fluorophore after excitation, leading to lower energy emission and a blue-shifted spectrum (Draganski et al., 2017; Lakowicz & Masters, 2008). Published molecular dynamics studies of PFOA binding to WT hLFABP indicates that a single PFOA ligand docks in a "head-out" mode, allowing the fluorinated tail to be stabilized by hydrophobic residues within the binding pocket, including F50 (Sheng et al., 2018; Zhang et al., 2013). Thus, at equilibrium PFOA may not sufficiently interact with the 28th residue located in the more solvated outer binding region nor the 63rd residue, located slightly deeper within the inner binding pocket than the eight carbon ligand is able to interact with. This is consistent with the lack of tryptophan mutant sensitivity to PFOA binding for the L28W and F63W mutants. As for the binding sensitive F50W hLFABP mutant, the shifted spectra data was fit to a dose–response model (Figure 2a), and a LOD of PFOA for the tryptophan was calculated to be 6.7 μM (2.8 ppm).

Affinity for PFAS ligands to WT and mutant hLFABP was measured by ANS displacement. First, binding affinity of the fluorescent dye ANS to WT and mutant hLFABP was assessed by measuring equilibrium fluorescence intensities for 1 μM protein samples titrated with increasing concentrations of ANS. Data were fit using nonlinear regression to determine the dissociation constants ($K_{d,ANS}$). Figure 2b presents fitted binding curves for WT and F50W, demonstrating no change in ANS affinity. Second, displacement of bound ANS was used to assess the binding of PFAS to hLFABP variants. Protein was first equilibrated with excess ANS, and the fluorescence spectra after PFAS titration was measured. As unlabeled ligand (PFAS) binds to the protein, ANS is displaced from hLFABP and fluorescence is quenched. Thus, the displacement of the ANS fluorophore was characterized as the percent loss in fluorescence. These values were then plotted as a function of PFAS concentration and fit to a sigmoidal dose–response model to obtain IC_{50} values. Figure 2c demonstrates PFOA binding to WT and F50W hLFABP. The IC_{50} values obtained in this way were then used to calculate an inhibition constant for PFAS ($K_{i,PFOA}$). All calculated inhibition constants, shown in Table 1, are in the micromolar range, and it can be inferred that the addition of all mutations does not negatively affect the binding of PFAS molecules.

To increase the sensitivity of the detection system, tryptophan was replaced with another solvatochromic fluorophore, 6-acryloyl-2-dimethylaminonaphthalene [Acrylodan]. Acrylodan is a prodan derivative that has been used to study protein conformational changes and ligand binding due to its high sensitivity to polarity (Gilardi et al., 1994; Hibbs et al., 2004; Hickey et al., 2017; Park et al., 2008). Conjugation of this probe to intestinal fatty acid binding protein has also been used to detect free fatty acid levels as well as membrane partitioning of fatty acids (Richieri et al., 1992; Simard et al., 2007).

The native cysteine at position 69 was first replaced with serine to ensure site specific thiol-fluorophore conjugation. This variant (C69S/F50W) resulted in inhibited dimerization as shown in Figure 3a. For labeling, the inner binding pocket-sensitive position for ligand binding was replaced with cysteine (F50C), resulting in a single cysteine containing hLFABP variant (C69S/F50C).

Proper refolding of C69S/F50C hLFABP after urea denaturation during acrylodan labeling was confirmed by comparing CD spectra before and after fluorophore conjugation (Figure 3b). The spectra for unlabeled and labeled proteins are essentially identical, with both samples containing 9.3% α-helix and 30.6% β-sheet as determined using the web-based server, BeStSel. BeStSel allows for characterization of eight different elements of protein structure to provide a more detailed description of protein secondary structure: regular α-helix, distorted α-helix, left twisted β-strand, relaxed β-strand,

TABLE 1 Binding parameters of PFOA for WT and F50W hLFABP as well as PFOA, PFOS, and PFHxS for C69S, C69S/F50W, and C69S/F50C hLFABP

	1,8-ANS	PFOA		PFOS		PFHxS	
	K_d (μM)	log (IC_{50})	K_i (μM)	log (IC_{50})	K_i (μM)	log (IC_{50})	K_i (μM)
WT	3.76 ± 0.61	1.62 ± 0.09	2.92 ± 0.60	–	–	–	–
F50W	2.97 ± 0.55	2.00 ± 0.26	5.66 ± 3.40	–	–	–	–
C69S	8.78 ± 3.28	1.60 ± 0.05	5.88 ± 0.75	1.00 ± 0.03	1.49 ± 0.12	1. 59 ± 0.05	5.77 ± 0.68
C69S/F50W	4.89 ± 1.70	2.18 ± 0.15	13.34 ± 4.68	1.60 ± 0.03	3.51 ± 0.25	1.89 ± 0.21	6.96 ± 3.37
C69S/F50C	5.86 ± 1.80	1.95 ± 0.15	9.29 ± 3.14	1.40 ± 0.04	2.65 ± 0.26	1.97 ± 0.27	9.90 ± 6.16

Note: These values were determined using displacement of the fluorophore 1,8-ANS. Error is reported as propagated SEM.

Abbreviations: 1,8-ANS, 1-anilinonaphthalene-8-sulfonic acid; hLFABP, human liver fatty acid binding protein; PFHxS, perfluorohexanesulfonic acid; PFOA, perfluorooctanoic acid; PFOS, perfluorooctanesulfonic acid.

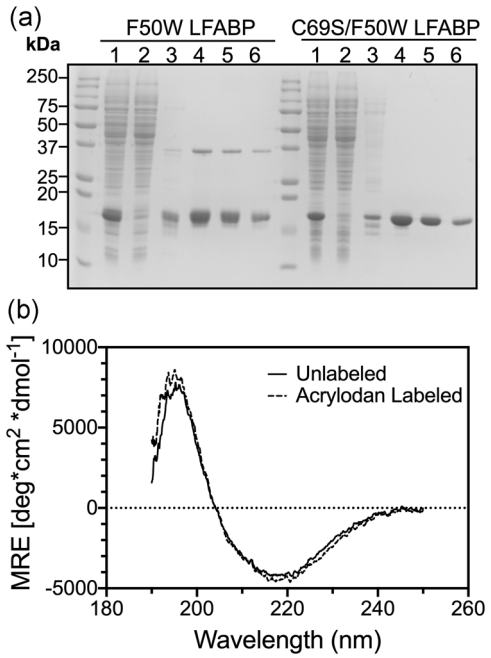

FIGURE 3 (a) SDS-PAGE gel of His-trap purified [Lanes] 1: whole cell lysate, 2: column flowthrough, 3–6: purified protein:: F50W hLFABP containing both monomer (~19 kDa) and formed dimer (~38 kDa) bands. F50W/C69S hLFABP containing only monomer band (~19 kDa). (b) CD spectra for unlabeled and acrylodan labeled C69S/F50C hLFABP. hLFABP, human liver fatty acid binding protein

right-twisted β-strand, parallel β-strand, turn, and other (Micsonai et al., 2018). Unlabeled and labeled C69S/F50C hLFABP showed identical compositions for all eight with 3%, 6.3%, 6.0%, 14.2%, 10.4%, 0.5%, 13.9%, and 45.6%, respectively, further confirming no change in protein structure occurs upon labeling.

After acrylodan conjugation, the protein was titrated with three PFAS molecules (PFOA, PFOS, and PFHxS) and equilibrium fluorescence spectra were measured in PBS buffer (pH 7.5) as well as in water samples taken from the Dell and Meadow Creek on the grounds of University of Virginia. For all three ligands, an increase in fluorescence as well as a blue shift in spectra were observed in both media systems suggesting this hLFABP variant is able to detect PFAS binding. Fitted data of the calculated spectra center of mass are shown in Figure 4a–c, with a larger dose–response shift in fluorescence upon titration of PFAS ligand to the tryptophan-containing protein (F50W; Figure 2a). Binding of 10 μM of the longer-chain PFAS molecules (PFOA and PFOS) to the acrylodan-based detection system resulted in a shifted center of mass of 10 nm in both PBS and surface water. This is more than a fourfold increase in signal as compared to PFOA binding to the tryptophan-based system, indicating improved sensitivity of detection using acrylodan. The estimated detection limit of PFOA in PBS was significantly improved with the substitution of acrylodan for tryptophan, with an LOD of 112 ppb and 10-fold reduction in protein needed for detection as compared to the F50W mutant. The calculated LOD for PFOS and PFHxS are 345 ppb and 1.09 ppm, respectively. Thus, use of acrylodan enhances LOD by an order of magnitude as compared to tryptophan, and enables detection directly from solution with a LOD within the reported range for other fluorescence and optical-based detection methods for PFAS. Figure 4d shows the fluorescence spectra of the acrylodan conjugated protein with and without bound PFOA in PBS buffer. Of note, not only is a shift in the center of mass upon PFOA binding observed, but also an increase in overall fluorescence intensity. While the sensitivity of the fluorescence increase upon binding does not result in the ppb LODs achieved utilizing the center of mass shift, this intensity change could potentially be useful for detection of PFAS at higher (ppm) concentrations.

Binding affinity for the acrylodan conjugated protein was assessed by using nonlinear regression to fit the data to both a one site and two site binding model. To correct for the negative response upon binding that is associated with a decrease in spectra center of mass, the binding occupancy was represented as the magnitude of the shift ($|\Delta X, _{cm}|$). The binding data conformed well only to the one site model (Figure 4e) which is consistent with previous studies suggesting PFOA is only capable of interacting with one binding site on the WT hLFABP (Sheng et al., 2016). Dissociation constants for PFOA, PFOS, and PFHxS were obtained from the one site model and are 1.18 ± 0.15, 1.73 ± 0.37, and 9.48 ± 2.20 μM, respectively. Binding affinity of PFHxS to the acrylodan labeled hLFABP variant is

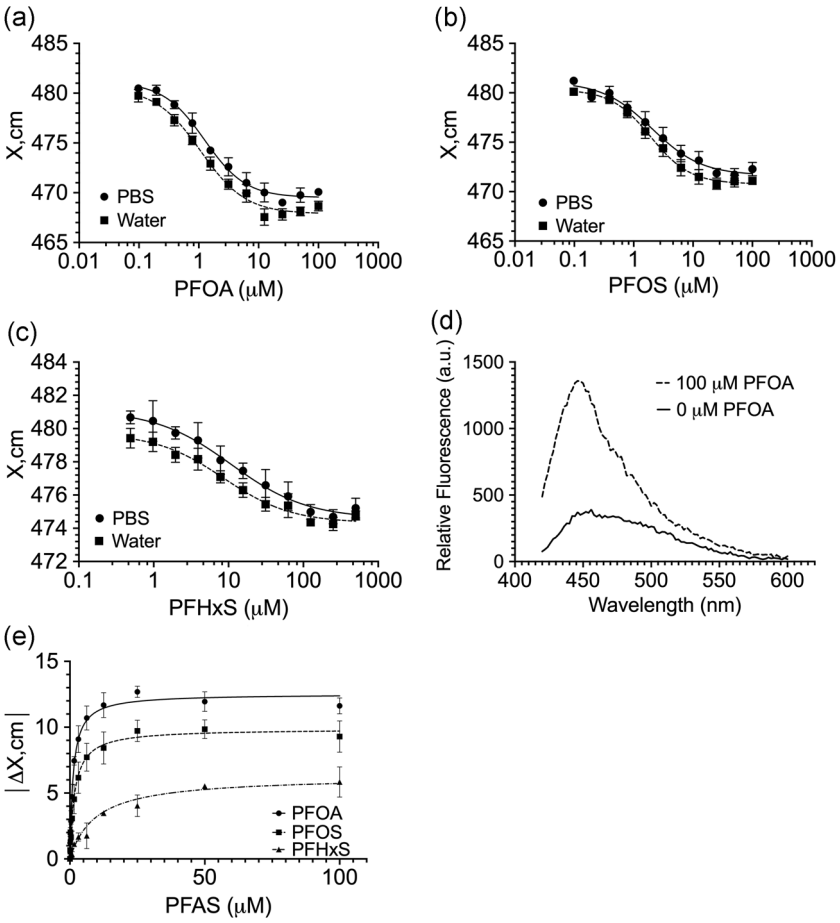

FIGURE 4 (a–c) Weighted average center of mass (*X*, cm) of fluorescence spectra for acrylodan conjugated C69S/F50C hLFABP (1 μM) after titration with PFOA (a), PFOS (b), and PFHxS (c) in PBS as well as in creek water. Blue shift in spectra upon increased PFAS concentration corresponds to binding and is visualized as a decrease in spectra center of mass (*X*, cm).:: (d) Fluorescence spectra of acrylodan conjugated C69S/F50C hLFABP (1 μM) with (dashed) and without (solid) PFOA in PBS. (e) Binding of PFAS to acrylodan conjugated C69S/F50C hLFABP (1 μM) fitted to a one site binding model with the fractional occupancy represented as the magnitude of change in center of mass (|Δ*X*, cm|). hLFABP, human liver fatty acid binding protein; PBS, phosphate-buffered saline; PFHxS, perfluorohexanesulfonic acid; PFOA, perfluorooctanoic acid; PFOS, perfluorooctanesulfonic acid

slightly weaker than the longer chain PFAS molecules PFOA and PFOS. This is consistent with binding affinities for hydrocarbon-chain containing fatty acids ligands, where binding affinity has been shown to increase with carbon chain length for C4–C11 molecules as their hydrophobic tails are able to fully extend in hLFABP's inner binding pocket (Zhang et al., 2013). Thus, it is possible that the shorter-chain PFHxS, when bound to the inner binding pocket, provides less available contact area for specific interactions and stabilization. This is also consistent with the higher LODs the acrylodan labeled sensor has for PFHxS. It is speculated that the shorter chain PFAS interacts less with the 50th residue resulting in decreased change in polarity as compared to the eight carbon PFOA and PFOS.

The specificity of the acrylodan-conjugated hLFABP variant was further tested by introducing the anionic surfactant, SDS, as a competitor for binding. Figure 5 shows the change in spectral center of mass for the protein sensor (1 μM) in PBS containing SDS (1 μM) upon titration of both PFOA and PFOS. The LODs for PFOA and PFOS were calculated to be 112 and 165 ppb, respectively.

While the magnitude of the fluorescence shift is decreased compared to system without SDS, the LOD values are comparable to those containing no additional surfactant. Thus, the engineered hLFABP sensor is capable of detecting both PFOA and PFOS at ppb levels in complex media containing anionic surfactants such as SDS that can act as inhibitors of binding.

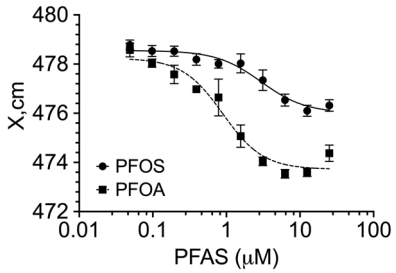

FIGURE 5 Weighted average center of mass (*X*, cm) of fluorescence spectra for acrylodan conjugated C69S/F50C hLFABP (1 μM) after titration with PFOA and PFOS in PBS containing SDS (1 μM). hLFABP, human liver fatty acid binding protein; PBS, phosphate-buffered saline; PFOA, perfluorooctanoic acid; PFOS, perfluorooctanesulfonic acid

Our approach is a useful initial step in development of protein-based biosensors to detect PFAS. Unlike PPARα and other mammalian receptors that bind PFAS, FABP is a robust scaffold that can be readily expressed and purified recombinantly in high yield versus extracted from mammalian tissues. Furthermore, direct detection from environmental samples is possible and detection is not impaired by the presence of interfering ligands such as SDS, unlike other approaches that require pretreatment to enrich PFAS or remove interfering substances. We also demonstrate the ability to modify the protein to

amplify signal and thus LOD, which we anticipate will enable further engineering approaches to approve affinity and LOD, as well as a complement to other ELISA- and QD-based biochemical PFAS detection strategies. Given that protein based sensors have been developed as green, effective alternatives for detection of many environmental contaminants including heavy metals, pharmaceuticals, and pesticides, LFABP could eventually serve as a useful scaffold for improved direct detection of PFAS in important solid and liquid matrices (Rodriguez-Mozaz et al., 2004; Thavarajah et al., 2020).

ACKNOWLEDGMENT

This study is supported by the University of Virginia and the Biotechnology Training Program NIGMS T32GM136615.

CONFLICT OF INTERESTS

The authors declare that there are no conflict of interests.

DATA AVAILABILITY STATEMENT

The data that support the findings of this study are available from the corresponding author upon reasonable request.

ORCID

Madison M. Mann http://orcid.org/0000-0002-7891-5185
Bryan W. Berger http://orcid.org/0000-0002-6135-8677

REFERENCES

Abraham, K., Mielke, H., Fromme, H., Völkel, W., Menzel, J., Peiser, M., Zepp, F., Willich, S. N., & Weikert, C. (2020). Internal exposure to perfluoroalkyl substances (PFASs) and biological markers in 101 healthy 1-year-old children: Associations between levels of perfluorooctanoic acid (PFOA) and vaccine response. *Archives of Toxicology*, *94*(6), 2131–2147. https://doi.org/10.1007/s00204-020-02715-4

Armstrong, L. E., & Guo, G. L. (2019). Understanding environmental contaminants' direct effects on non-alcoholic fatty liver disease progression. *Current Environmental Health Reports*, *6*(3), 95–104. https://doi.org/10.1007/s40572-019-00231-x

Atshaves, B. P., Martin, G. G., Hostetler, H. A., McIntosh, A. L., Kier, A. B., & Schroeder, F. (2010). Liver fatty acid binding protein and obesity. *The Journal of Nutritional Biochemistry*, *21*(11), 1015–1032. https://doi.org/10.1016/j.jnutbio.2010.01.005

Blaine, A. C., Rich, C. D., Hundal, L. S., Lau, C., Mills, M. A., Harris, K. M., & Higgins, C. P. (2013). Uptake of perfluoroalkyl acids into edible crops via land applied biosolids: Field and greenhouse studies. *Environmental Science & Technology*, *47*(24), 14062–14069. https://doi.org/10.1021/es403094q

Blaine, A. C., Rich, C. D., Sedlacko, E. M., Hyland, K. C., Stushnoff, C., Dickenson, E. R. V., & Higgins, C. P. (2014). Perfluoroalkyl acid uptake in lettuce (*Lactuca sativa*) and strawberry (*Fragaria ananassa*) irrigated with reclaimed water. *Environmental Science & Technology*, *48*(24), 14361–14368. https://doi.org/10.1021/es504150h

Bulka, C. M., Avula, V., & Fry, R. C. (2021). Associations of exposure to perfluoroalkyl substances individually and in mixtures with persistent infections: Recent findings from NHANES 1999–2016. *Environmental Pollution*, *275*, 116619. https://doi.org/10.1016/j.envpol.2021.116619

Butt, C. M., Muir, D. C. G., & Mabury, S. A. (2014). Biotransformation pathways of fluorotelomer-based polyfluoroalkyl substances: A review. *Environmental Toxicology and Chemistry*, *33*(2), 243–267. https://doi.org/10.1002/etc.2407

Cai, J., Lücke, C., Chen, Z., Qiao, Y., Klimtchuk, E., & Hamilton, J. A. (2012). Solution structure and backbone dynamics of human liver fatty acid binding protein: Fatty acid binding revisited. *Biophysical Journal*, *102*(11), 2585–2594. https://doi.org/10.1016/j.bpj.2012.04.039

Calafat, A. M., Kuklenyik, Z., Caudill, S. P., Reidy, J. A., & Needham, L. L. (2006). Perfluorochemicals in pooled serum samples from United States residents in 2001 and 2002. *Environmental Science & Technology*, *40*(7), 2128–2134. https://doi.org/10.1021/es0517973

Calafat, A. M., Kuklenyik, Z., Reidy, J. A., Caudill, S. P., Tully, J. S., & Needham, L. L. (2007). Serum concentrations of 11 polyfluoroalkyl compounds in the U.S. population: Data from the National Health and Nutrition Examination Survey (NHANES) 1999–2000. *Environmental Science & Technology*, *41*(7), 2237–2242. https://doi.org/10.1021/es062686m

Carlson, G. L., & Tupper, S. (2020). Ski wax use contributes to environmental contamination by per- and polyfluoroalkyl substances. *Chemosphere*, *261*, 128078. https://doi.org/10.1016/j.chemosphere.2020.128078

Cheng, W., & Ng, C. A. (2018). Predicting relative protein affinity of novel per- and polyfluoroalkyl substances (PFASs) by an efficient molecular dynamics approach. *Environmental Science & Technology*, *52*(14), 7972–7980. https://doi.org/10.1021/acs.est.8b01268

Cousins, I. T., Vestergren, R., Wang, Z., Scheringer, M., & McLachlan, M. S. (2016). The precautionary principle and chemicals management: The example of perfluoroalkyl acids in groundwater. *Environment International*, *94*, 331–340. https://doi.org/10.1016/j.envint.2016.04.044

Dauchy, X., Boiteux, V., Bach, C., Rosin, C., & Munoz, J.-F. (2017). Per- and polyfluoroalkyl substances in firefighting foam concentrates and water samples collected near sites impacted by the use of these foams. *Chemosphere*, *183*, 53–61. https://doi.org/10.1016/j.chemosphere.2017.05.056

Dauchy, X., Boiteux, V., Colin, A., Hémard, J., Bach, C., Rosin, C., & Munoz, J.-F. (2019). Deep seepage of per- and polyfluoroalkyl substances through the soil of a firefighter training site and subsequent groundwater contamination. *Chemosphere*, *214*, 729–737. https://doi.org/10.1016/j.chemosphere.2018.10.003

Draganski, A. R., Friedman, J. M., & Ludescher, R. D. (2017). Solvent-slaved dynamic processes observed by tryptophan phosphorescence of human serum albumin. *Biophysical Journal*, *112*(5), 881–891. https://doi.org/10.1016/j.bpj.2016.12.048

Fang, C., Zhang, X., Dong, Z., Wang, L., Megharaj, M., & Naidu, R. (2018). Smartphone app-based/portable sensor for the detection of fluoro-surfactant PFOA. *Chemosphere*, *191*, 381–388. https://doi.org/10.1016/j.chemosphere.2017.10.057

Favreau, P., Poncioni-Rothlisberger, C., Place, B. J., Bouchex-Bellomie, H., Weber, A., Tremp, J., Field, J. A., & Kohler, M. (2017). Multianalyte profiling of per- and polyfluoroalkyl substances (PFASs) in liquid commercial products. *Chemosphere*, *171*, 491–501. https://doi.org/10.1016/j.chemosphere.2016.11.127

Feng, H., Wang, N., Tran, T. T., Yuan, L., Li, J., & Cai, Q. (2014). Surface molecular imprinting on dye–(NH_2)–SiO_2 NPs for specific recognition and direct fluorescent quantification of perfluorooctane sulfonate. *Sensors and Actuators B: Chemical*, *195*, 266–273. https://doi.org/10.1016/j.snb.2014.01.036

Fenton, S. E., Ducatman, A., Boobis, A., DeWitt, J. C., Lau, C., Ng, C., Smith, J. S., & Roberts, S. M. (2021). Per- and polyfluoroalkyl substance toxicity and human health review: current state of knowledge and strategies for informing future research. *Environmental Toxicology and Chemistry*, *40*(3), 606–630. https://doi.org/10.1002/etc.4890

Gilardi, G., Zhou, L. Q., Hibbert, L., & Cass, A. E. (1994). Engineering the maltose binding protein for reagentless fluorescence sensing.

Analytical Chemistry, *66*(21), 3840–3847. https://doi.org/10.1021/ac00093a047

Hagan, R. M., Worner-Gibbs, J., & Wilton, D. C. (2005). Tryptophan insertion mutagenesis of liver fatty acid-binding protein: L28W mutant provides important insights into ligand binding and physiological function. *Journal of Biological Chemistry*, *280*(3), 1782–1789. https://doi.org/10.1074/jbc.M407131200

Harding-Marjanovic, K. C., Houtz, E. F., Yi, S., Field, J. A., Sedlak, D. L., & Alvarez-Cohen, L. (2015). Aerobic biotransformation of fluorotelomer thioether amido sulfonate (Lodyne) in AFFF-amended microcosms. *Environmental Science & Technology*, *49*(13), 7666–7674. https://doi.org/10.1021/acs.est.5b01219

Hibbs, R. E., Talley, T. T., & Taylor, P. (2004). Acrylodan-conjugated cysteine side chains reveal conformational state and ligand site locations of the acetylcholine-binding protein. *Journal of Biological Chemistry*, *279*(27), 28483–28491. https://doi.org/10.1074/jbc.M403713200

Hickey, J. M., Sahni, N., Chaudhuri, R., D'Souza, A., Metters, A., Joshi, S. B., Russell Middaugh, C., & Volkin, D. B. (2017). Effect of acrylodan conjugation and forced oxidation on the structural integrity, conformational stability, and binding activity of a glucose binding protein SM4 used in a prototype continuous glucose monitor. *Protein Science*, *26*(3), 527–535. https://doi.org/10.1002/pro.3102

Hoffman, K., Webster, T. F., Weisskopf, M. G., Weinberg, J., & Vieira, V. M. (2010). Exposure to polyfluoroalkyl chemicals and attention deficit/hyperactivity disorder in U.S. Children 12–15 years of age. *Environmental Health Perspectives*, *118*(12), 1762–1767. https://doi.org/10.1289/ehp.1001898

Hu, X., Liu, Y., Yang, R., Jiang, Y., Meng, M., Liu, Z., Ni, L., Wu, W., & Liu, H. (2020). Adsorption for perfluorooctanoic acid with graphitic-phase carbon nitride and its HPLC fluorescence determination. *The Canadian Journal of Chemical Engineering*, *98*(1), 394–403. https://doi.org/10.1002/cjce.23625

Jiao, Z., Li, J., Mo, L., Liang, J., & Fan, H. (2018). A molecularly imprinted chitosan doped with carbon quantum dots for fluorometric determination of perfluorooctane sulfonate. *Microchimica Acta*, *185*(10), 473. https://doi.org/10.1007/s00604-018-2996-y

Karimian, N., Stortini, A. M., Moretto, L. M., Costantino, C., Bogialli, S., & Ugo, P. (2018). Electrochemosensor for trace analysis of perfluorooctanesulfonate in water based on a molecularly imprinted poly(o-phenylenediamine) polymer. *ACS Sensors*, *3*(7), 1291–1298. https://doi.org/10.1021/acssensors.8b00154

Kazemi, R., Potts, E. I., & Dick, J. E. (2020). Quantifying interferent effects on molecularly imprinted polymer sensors for per- and polyfluoroalkyl substances (PFAS). *Analytical Chemistry*, *92*(15), 10597–10605. https://doi.org/10.1021/acs.analchem.0c01565

Kotthoff, M., Müller, J., Jürling, H., Schlummer, M., & Fiedler, D. (2015). Perfluoroalkyl and polyfluoroalkyl substances in consumer products. *Environmental Science and Pollution Research International*, *22*(19), 14546–14559. https://doi.org/10.1007/s11356-015-4202-7

Lakowicz, J. R., & Masters, B. R. (2008). Principles of fluorescence spectroscopy, third edition. *Journal of Biomedical Optics*, *13*(2), 029901. https://doi.org/10.1117/1.2904580

Looker, C., Luster, M. I., Calafat, A. M., Johnson, V. J., Burleson, G. R., Burleson, F. G., & Fletcher, T. (2014). Influenza vaccine response in adults exposed to perfluorooctanoate and perfluorooctanesulfonate. *Toxicological Sciences*, *138*(1), 76–88. https://doi.org/10.1093/toxsci/kft269

Mamsen, L. S., Björvang, R. D., Mucs, D., Vinnars, M.-T., Papadogiannakis, N., Lindh, C. H., Andersen, C. Y., & Damdimopoulou, P. (2019). Concentrations of perfluoroalkyl substances (PFASs) in human embryonic and fetal organs from first, second, and third trimester pregnancies. *Environment International*, *124*, 482–492. https://doi.org/10.1016/j.envint.2019.01.010

Markiewicz, B. N., Mukherjee, D., Troxler, T., & Gai, F. (2016). Utility of 5-cyanotryptophan fluorescence as a sensitive probe of protein hydration. *The Journal of Physical Chemistry B*, *120*(5), 936–944. https://doi.org/10.1021/acs.jpcb.5b12233

Micsonai, A., Wien, F., Bulyáki, É., Kun, J., Moussong, É., Lee, Y.-H., Goto, Y., Réfrégiers, M., & Kardos, J. (2018). BeStSel: A web server for accurate protein secondary structure prediction and fold recognition from the circular dichroism spectra. *Nucleic Acids Research*, *46*(W1), W315–W322. https://doi.org/10.1093/nar/gky497

Mora, A. M., Fleisch, A. F., Rifas-Shiman, S. L., Baidal, J. W., Pardo, L., Webster, T. F., Calafat, A. M., Ye, X., Oken, E., & Sagiv, S. K. (2018). Early life exposure to per- and polyfluoroalkyl substances and mid-childhood lipid and alanine aminotransferase levels. *Environment International*, *111*, 1–13. https://doi.org/10.1016/j.envint.2017.11.008

Mora, A. M., Oken, E., Rifas-Shiman, S. L., Webster, T. F., Gillman, M. W., Calafat, A. M., Ye, X., & Sagiv, S. K. (2017). Prenatal exposure to perfluoroalkyl substances and adiposity in early and mid-childhood. *Environmental Health Perspectives*, *125*(3), 467–473. https://doi.org/10.1289/EHP246

Park, H. Y., Kim, S. A., Korlach, J., Rhoades, E., Kwok, L. W., Zipfel, W. R., Waxham, M. N., Webb, W. W., & Pollack, L. (2008). Conformational changes of calmodulin upon Ca2+ binding studied with a microfluidic mixer. *Proceedings of the National Academy of Sciences*, *105*(2), 542–547. https://doi.org/10.1073/pnas.0710810105

Prendergast, F. G., Meyer, M., Carlson, G. L., Iida, S., & Potter, J. D. (1983). Synthesis, spectral properties, and use of 6-acryloyl-2-dimethylaminonaphthalene (Acrylodan). A thiol-selective, polarity-sensitive fluorescent probe. *The Journal of Biological Chemistry*, *258*(12), 7541–7544.

Richieri, G. V., Ogata, R. T., & Kleinfeld, A. M. (1992). A fluorescently labeled intestinal fatty acid binding protein. Interactions with fatty acids and its use in monitoring free fatty acids. *The Journal of Biological Chemistry*, *267*(33), 23495–23501.

Robel, A. E., Marshall, K., Dickinson, M., Lunderberg, D., Butt, C., Peaslee, G., Stapleton, H. M., & Field, J. A. (2017). Closing the mass balance on fluorine on papers and textiles. *Environmental Science & Technology*, *51*(16), 9022–9032. https://doi.org/10.1021/acs.est.7b02080

Rodriguez-Mozaz, S., Reder, S., Lopez de Alda, M., Gauglitz, G., & Barceló, D. (2004). Simultaneous multi-analyte determination of estrone, isoproturon and atrazine in natural waters by the RIver ANAlyser (RIANA), an optical immunosensor. *Biosensors and Bioelectronics*, *19*(7), 633–640. https://doi.org/10.1016/S0956-5663(03)00255-0

Royer, C. A. (2006). Probing protein folding and conformational transitions with fluorescence. *Chemical Reviews*, *106*(5), 1769–1784. https://doi.org/10.1021/cr0404390

Schaider, L. A., Balan, S. A., Blum, A., Andrews, D. Q., Strynar, M. J., Dickinson, M. E., Lunderberg, D. M., Lang, J. R., & Peaslee, G. F. (2017). Fluorinated compounds in U.S. fast food packaging. *Environmental Science & Technology Letters*, *4*(3), 105–111. https://doi.org/10.1021/acs.estlett.6b00435

Sharma, A., & Sharma, A. (2011). Fatty acid induced remodeling within the human liver fatty acid-binding protein. *The Journal of Biological Chemistry*, *286*(36), 31924–31928. https://doi.org/10.1074/jbc.M111.270165

Sheng, N., Cui, R., Wang, J., Guo, Y., Wang, J., & Dai, J. (2018). Cytotoxicity of novel fluorinated alternatives to long-chain perfluoroalkyl substances to human liver cell line and their binding capacity to human liver fatty acid binding protein. *Archives of Toxicology*, *92*(1), 359–369. https://doi.org/10.1007/s00204-017-2055-1

Sheng, N., Li, J., Liu, H., Zhang, A., & Dai, J. (2016). Interaction of perfluoroalkyl acids with human liver fatty acid-binding protein. *Archives of Toxicology*, *90*(1), 217–227. https://doi.org/10.1007/s00204-014-1391-7

Shoemaker, J. D. T. (2020). Method 537.1 determination of selected per- and polyflourinated alkyl substances in drinking water by solid phase extraction and liquid chromatography/tandem mass spectrometry (LC/MS/MS). U.S. Environmental Protection Agency.

Simard, J. R., Kamp, F., & Hamilton, J. A. (2007). Acrylodan-labeled intestinal fatty acid-binding protein to measure concentrations of unbound fatty acids. *Methods in Membrane Lipids*, *400*, 27–43. https://doi.org/10.1007/978-1-59745-519-0_3

Stanifer, J. W., Stapleton, H. M., Souma, T., Wittmer, A., Zhao, X., & Boulware, L. E. (2018). Perfluorinated chemicals as emerging environmental threats to kidney health: A scoping review. *Clinical Journal of the American Society of Nephrology*, *13*(10), 1479–1492. https://doi.org/10.2215/CJN.04670418

Steenland, K., Fletcher, T., & Savitz, D. A. (2010). Epidemiologic evidence on the health effects of perfluorooctanoic acid (PFOA). *Environmental Health Perspectives*, *118*(8), 1100–1108. https://doi.org/10.1289/ehp.0901827

Steenland, K., Tinker, S., Frisbee, S., Ducatman, A., & Vaccarino, V. (2009). Association of perfluorooctanoic acid and perfluorooctane sulfonate with serum lipids among adults living near a chemical plant. *American Journal of Epidemiology*, *170*(10), 1268–1278. https://doi.org/10.1093/aje/kwp279

Thavarajah, W., Verosloff, M. S., Jung, J. K., Alam, K. K., Miller, J. D., Jewett, M. C., Young, S. L., & Lucks, J. B. (2020). A primer on emerging field-deployable synthetic biology tools for global water quality monitoring. *Npj Clean Water*, *3*(1), 1–10. https://doi.org/10.1038/s41545-020-0064-8

Thompson, J., Winter, N., Terwey, D., Bratt, J., & Banaszak, L. (1997). The crystal structure of the liver fatty acid-binding protein: A complex with two bound oleates. *Journal of Biological Chemistry*, *272*(11), 7140–7150. https://doi.org/10.1074/jbc.272.11.7140

United States Environmental Protection Agency Office of Water (4304T) Health and Ecological Criteria Division. (2016a). *Drinking water health advisory for perfluorooctane sulfonate (PFOS)* (EPA Document Number 822-R-16-004). US EPA Federal Registry.

United States Environmental Protection Agency Office of Water (4304T) Health and Ecological Criteria Division. (2016b). *Drinking water health advisory for perfluorooctanoic acid (PFOA)* (EPA Document Number: 822-R-16-005). US EPA Federal Registry.

Velkov, T., Chuang, S., Wielens, J., Sakellaris, H., Charman, W. N., Porter, C. J. H., & Scanlon, M. J. (2005). The interaction of lipophilic drugs with intestinal fatty acid-binding protein. *Journal of Biological Chemistry*, *280*(18), 17769–17776. https://doi.org/10.1074/jbc.M410193200

Vuong, A. M., Yolton, K., Webster, G. M., Sjödin, A., Calafat, A. M., Braun, J. M., Dietrich, K. N., Lanphear, B. P., & Chen, A. (2016). Prenatal polybrominated diphenyl ether and perfluoroalkyl substance exposures and executive function in school-age children. *Environmental Research*, *147*, 556–564. https://doi.org/10.1016/j.envres.2016.01.008

Wang, Z., DeWitt, J. C., Higgins, C. P., & Cousins, I. T. (2017). A never-ending story of per- and polyfluoroalkyl substances (PFASs)? *Environmental Science & Technology*, *51*(5), 2508–2518. https://doi.org/10.1021/acs.est.6b04806

Washino, N., Saijo, Y., Sasaki, S., Kato, S., Ban, S., Konishi, K., Ito, R., Nakata, A., Iwasaki, Y., Saito, K., Nakazawa, H., & Kishi, R. (2009). Correlations between prenatal exposure to perfluorinated chemicals and reduced fetal growth. *Environmental Health Perspectives*, *117*(4), 660–667. https://doi.org/10.1289/ehp.11681

Xia, W., Wan, Y.-J., Wang, X., Li, Y.-Y., Yang, W.-J., Wang, C.-X., & Xu, S. (2011). Sensitive bioassay for detection of PPARα potentially hazardous ligands with gold nanoparticle probe. *Journal of Hazardous Materials*, *192*(3), 1148–1154. https://doi.org/10.1016/j.jhazmat.2011.06.023

Zhang, L., Ren, X.-M., & Guo, L.-H. (2013). Structure-based investigation on the interaction of perfluorinated compounds with human liver fatty acid binding protein. *Environmental Science & Technology*, *47*(19), 11293–11301. https://doi.org/10.1021/es4026722

How to cite this article: Mann, M. M., Tang, J. D., & Berger, B. W. (2022). Engineering human liver fatty acid binding protein for detection of poly- and perfluoroalkyl substances. *Biotechnology and Bioengineering*, 119, 513–522. https://doi.org/10.1002/bit.27981